Journal of Neuroscience Methods 392 (2023) 109853

Contents lists available at ScienceDirect

Journal of Neuroscience Methods

journal homepage: www.elsevier.com/locate/jneumeth

Real-Time Semi-Automated and Automated Voxel Placement using fMRI Targets for Repeated Acquisition Magnetic Resonance Spectroscopy☆

James H. Bishop [a,b], Andrew Geoly [a], Naushaba Khan [a], Claudia Tischler [a], Ruben Krueger [a], Poorvi Keshava [d], Heer Amin [a], Laima Baltusis [c], Hua Wu [c], David Spiegel [a], Nolan Williams [a], Matthew D. Sacchet [d,*]

[a] Department of Psychiatry and Behavioral Sciences, Stanford University, Stanford, CA, USA
[b] Department of Radiology, Stanford University, Stanford, CA, USA
[c] Center for Cognitive and Neurobiological Imaging, Stanford University, Stanford, CA, USA
[d] Meditation Research Program, Department of Psychiatry, Massachusetts General Hospital, Harvard Medical School, Boston, MA, USA

ARTICLE INFO

Keywords:
Magnetic resonance spectroscopy (MRS)
Voxel placement
Data acquisition
Reliability
Reproducibility
Longitudinal

ABSTRACT

Background: Currently, magnetic resonance spectroscopy (MRS) is dependent on the investigative team to *manually* prescribe, or demarcate, the desired tissue volume-of-interest. The need for a new method to automate precise voxel placements is warranted to improve the utility and interpretability of MRS data.
New Method: We propose and validate robust and real-time methods to automate MRS voxel placement using functionally defined coordinates within the prefrontal cortex. Data were collected and analyzed using two independent prospective studies: 1) two independent imaging days with each consisting of a multi-session sandwich design (MRS data only collected on one of the days determined based on scan time) and 2) a longitudinal design. Participants with fibromyalgia syndrome (N = 50) and major depressive disorder (N = 35) underwent neuroimaging. MRS acquisitions were acquired at 3-tesla. Evaluation of the reproducibility of spatial location and tissue segmentation was assessed for: 1) manual, 2) semi-automated, and 3) automated voxel prescription approaches
Results: Variability of voxel grey and white matter tissue composition was reduced using automated placement protocols. Spatially, post- to pre-voxel center-of-gravity distance was reduced and voxel overlap increased significantly across datasets using automated compared to manual procedures
Comparison with existing methods: Manual prescription, the current standard in the field, can produce inconsistent data across repeated acquisitions. Using automated voxel placement, we found reduced variability and more consistent voxel placement across multiple acquisitions
Conclusions: These results demonstrate the within subject reliability and reproducibility of a method for reducing variability introduced by spatial inconsistencies during MRS acquisitions. The proposed method is a meaningful advance toward improved consistency of MRS data in neuroscience and can be utilized for multi-session and longitudinal studies.

1. Introduction

Magnetic resonance spectroscopy (MRS) is a non-invasive brain imaging approach capable of quantifying diverse metabolic and biochemical processes including specific neurotransmitters (Stanley and Raz, 2018; Schur et al., 2016). MRS generally requires the user to prospectively delineate the tissue volumes-of-interest (VOI) warranting new and easy to use methods for reliable and reproducible data collection. Conducting investigations without precisely placed voxels limits the utility and interpretability of MRS data for use in evaluating complex

Abbreviations: VOI, volumes-of-interest; MEGA-PRESS, MEshcher-Garwood Point RESolved Spectroscopy; FLIRT, FSL LInear Registration Tools (FLIRT); DSC, dice similarity coefficient.

☆ Present Address: Meditation Research Program, Department of Psychiatry, Massachusetts General Hospital, Harvard Medical School, Boston, MA, USA

* Correspondence to: Athinoula A. Martinos Center for Biomedical Imaging, CNY Building #149, 149 13th St., Charlestown, MA 02129-4522, USA.
E-mail address: msacchet@mgh.harvard.edu (M.D. Sacchet).

https://doi.org/10.1016/j.jneumeth.2023.109853
Received 15 May 2022; Received in revised form 2 April 2023; Accepted 6 April 2023
Available online 7 April 2023

disorders and interventions.

Precision of MRS VOIs is generally reliant on the clinical or investigative team and their neuroanatomical expertise. Even with appropriate expertise, consistent voxel prescription can be further challenged by inter-subject anatomical variability. These factors may be compounded as the size of the VOI decreases, and with it, the related biochemical measurements of interest (Oz et al., 2020). Standard MRS VOI placement approaches are especially problematic for multi-center, cross--sectional, and repeated measures trials that involve data collection by multiple users over time. Indeed, long-term projects often have turnover in research staff and there is often a broad range in user experience levels. Taken together, these factors contribute to increased variability and decreased consistency of voxel placement and thus weaken the validity of MRS measurements.

Inter-individual anatomical variability is a challenge for voxel prescription. Even if spatial consistency is achieved manually by the MRI system operator using only grossly visible landmarks, this does not ensure that the user is measuring the *functionally* analogous region across participants. Many of the current approaches for VOI placement ignore the functional and/or cytoarchitectural heterogeneity across brain structures because they are not visualizable. For context, prefrontal structures such as the dorsolateral prefrontal cortex (DLPFC) are highly variable across participants and have undergone iterations of refinement since the original Brodmann parcellations (Rajkowska and Goldman-Rakic, 1995; von Economo and Koskinas, 1925; Sarkissov et al., 1955; Brodmann, 1909). This further confounds the utility of MRS to investigate complex disorders where the neural circuitry involved may not demonstrate grossly observable pathology. While integration of real-time functional MRI tasks for guiding voxel prescription has been developed, these techniques require robust and validated tasks that must be implemented in a short timeframe. For example, the use of functional localizers and task-based methods such as finger tapping, the n-back task, or visual stimuli have been use to guide voxel placement in the motor, prefrontal, and visual cortices respectively (Koush et al., 2019; Yasen et al., 2017; Koush et al., 2011). These methods are promising, however, an expansion of the approach to enable coordinate-based prescription across participants is warranted for placement in regions that lack definitive task-based activation paradigms or to ensure consistent placement across repeated MRI visits/scans without needing to reacquire localizers. Coordinate based voxel prescription enables a wide array of methodological flexibility that may increase the reliability within participants and across studies.

Coordinate based anatomical voxel prescription methods have been developed to overcome the variability introduced by manual voxel placement, but the current approaches have yet to integrate placement with functional targets or in a within participant registration paradigm for repeated acquisition consistency. For example, several methods have been proposed that afford user independent automated VOI placement that utilize brain co-registration (alignment) methods. These rely on either affine (linear) or b-spline (non-linear) brain co-registration that align a subject's anatomical scan to a standard brain atlas or template during the imaging session (Park et al., 2018). The registration parameters are then used to quantitatively identify template-to-individual voxel placement coordinates which are then input by the user into the scanner acquisition software. An advantage of affine approaches is that they are fast, require minimal computational resources (which may be helpful in real-time data acquisition contexts), and the performance is optimal for within subject coregistration, however, this requires repeated acquisition paradigms.

Thus, the use of MRS as a neuroscientific tool for the identification of neurochemical concentrations will benefit from methods that can be conducted quickly by study personnel, are reliably prescribed in an automated fashion, applied on an individual subject basis, and are reproducible across longitudinal, multi-acquisition, and repeated measurements. The methods used to determine VOIs, whether based on function, structure, or otherwise, are ultimately dependent on researcher or clinician preference and the scientific/clinical question. Here we provide a methodological framework for the automation of repeated-measure and longitudinal acquisition of MRS voxels in a heterogenous functional brain region, the dorsolateral prefrontal cortex (DLPFC). In this investigation, we examine two iterations of our approach which we term "semi-automated" and "automated" based on the amount of user input across repeated measure and longitudinal acquisitions as well as a manual MRS voxel prescription in two independent clinical datasets. We implemented fast b-spline (affine) registration of anatomical images and co-registration of an individual-based functional (fMRI) coordinate of interest to center the VOI in a clinically relevant portion of the left DLPFC (L-DLPFC). Compared to standard manual voxel prescription, we aimed to demonstrate that less user input via enhanced automation would reduce spatial and tissue variability across repeated MRS acquisitions in voxels of different sizes within the L-DLPFC. We implemented field-standard segmentation approaches, including those packaged within Freesurfer (Fischl et al., 2002) and Statistical Parametric Mapping (SPM) (Ashburner and Friston, 2005), to evaluate tissue fraction across prescription pipelines. To quantify the consistency of voxel placements, we calculated Euclidean distance from the center-of-gravity coordinates across scans, in addition to determining the similarity of MRS voxels using an overlap coefficient across repeated MRS acquisitions.

2. Methods

2.1. Participant recruitment and evaluation

Participants were recruited as part of two separate studies. Both studies were approved by the Stanford University Institutional Review Board (IRB) and participants provided informed consent. All procedures were in compliance with the Declaration of Helsinki. Prior to imaging, participants were evaluated for standard MRI contraindications, in-person, by study coordinators and a study physician and provided informed consent.

Study A was used to evaluate the voxel placement between independent MRI sessions spaced one hour apart. In brief, 50 participants with fibromyalgia syndrome, a chronic pain disorder, first underwent a baseline MRI (MRI #1) followed by two separate experimental days - each with two independent MRI scans (MRI #2–5) sandwiched between transcranial magnetic stimulation treatment (Fig. 1). Resting state functional scans were acquired at the baseline MRI (MRI #1), analyzed, and the identified L-DLPFC cluster coordinate was used during each of the subsequent MRIs (MRI #2–5) for automated voxel prescription. MRI sessions were approximately 1-hours and included a combination of structural, chemical, and functional acquisitions. GABA-edited MEGA-PRESS (MEshcher-Garwood Point RESolved Spectroscopy) and broad spectra Optimized-PRESS MRS sequences were collected pre- and post-TMS MRI sessions only. Imaging parameters are described in greater detail below. A total of 50 pre-/post-MEGA-PRESS and 50 pre-/post-Optimized-PRESS scans were collected culminating in 200 total acquisitions.

Study B was conducted in a treatment resistant major depressive disorder population undergoing resting state functional connectivity guided TMS therapy. The paradigm was used to evaluate within-subject voxel placements between three independent MRI sessions at the following timepoints: (Stanley and Raz, 2018) baseline (MRI #1), (Schur et al., 2016) one-week (MRI #2), and (Oz et al., 2020) one-month (MRI #3, Fig. 1). Resting state functional scans were collected and analyzed during the baseline MRI (MRI #1) and thus manual DLPFC voxel placement was instituted during this timepoint. The identified L-DLPFC resting state cluster coordinate was then used to guide the voxel placement during the one-week and one-month MRI evaluations (MRI #2–3). A combination of structural, chemical, and functional imaging was collected at all MRI sessions. MEGA-PRESS MRS for the 38 participants was acquired at each of the three timepoints detailed above and

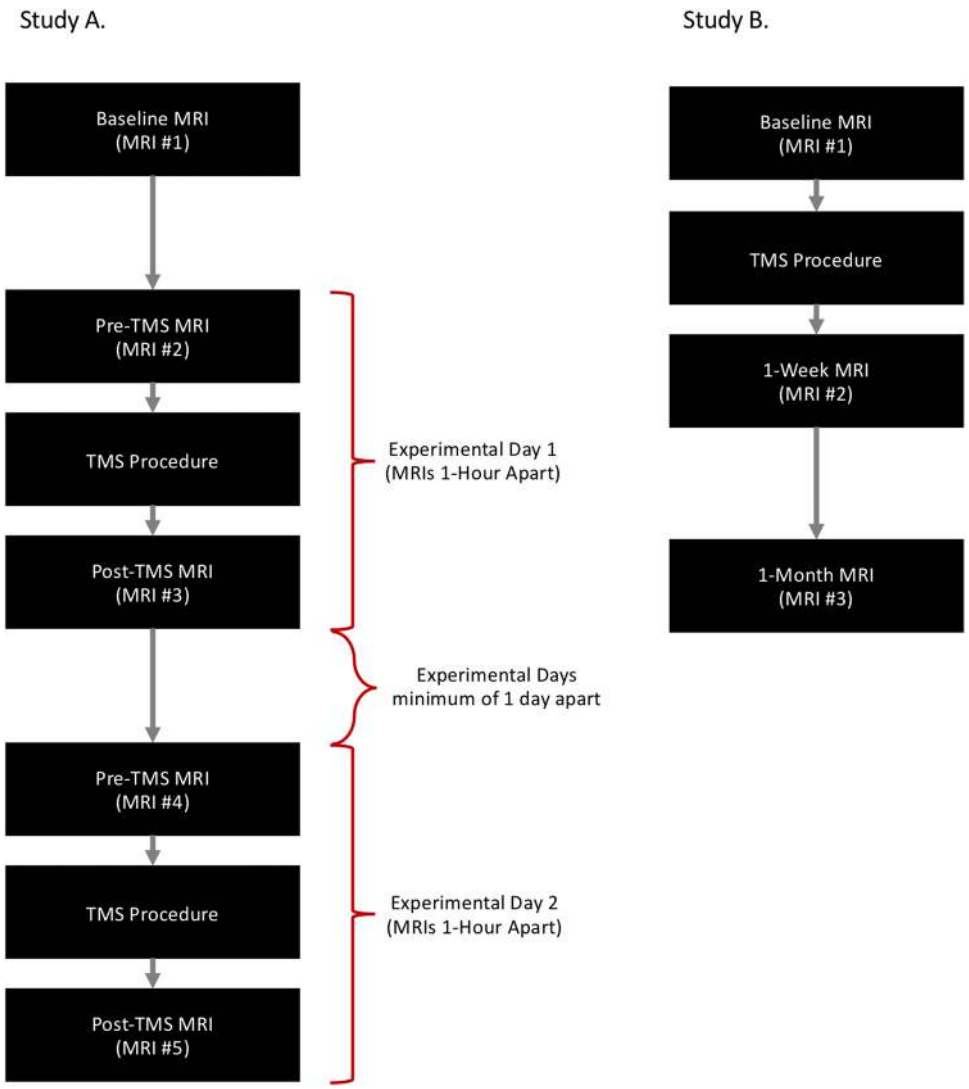

Fig. 1. Experimental Design: Study A (left) timeline demonstrating a repeated-acquisition sandwich design where there were two different imaging days consisting of two independent MRI scans sandwiched between a TMS intervention. Study B (right) demonstrates a longitudinal imaging design with three independent scans at varying follow-up timeframes: baseline, one-week, and one-month MRI visits.

included 114 total MEGA-PRESS acquisitions. Imaging parameters are described in greater detail below.

2.2. MRI data acquisition

MRI data were obtained using a research dedicated 3.0 T General Electric Discovery MR750 instrument with a Nova Medical 32-channel head coil. Acquisition parameters were identical across both studies (i.e., studies A & B) and included a combination of: structural, chemical, and functional acquisitions. Whole-brain structural imaging consisted of a 0.9 mm^3 three-dimensional T1w Magnetization Prepared - Rapid Gradient Echo (MPRAGE) sequence. Whole-brain high resolution fMRI (resting state) was collected using a simultaneous multi-slice EPI sequence with the following parameters: echo time (TE) = 30 ms, repetition time (TR) = 2 s, flip angle = 77°, slice thickness = 1.8 mm, and FOV = 230 mm. Broad spectra and GABA+ MRS data were collected using Optimized-PRESS (Tran et al., 2000; Webb et al., 1994; Bodenhausen et al., 1969) and MEGA-PRESS (Mescher et al., 1998) sequences respectively within the left DLPFC (L-DLPFC). MEGA-PRESS sequence parameters included: voxel size = 20×20×20 mm (volume = 8 cm3) TE = 68 ms; TR = 2 s; editing pulses applied at 1.9 ppm (ON) and 7.46 ppm (OFF) for a total acquisition time of ~10 min. Optimized-PRESS sequence parameters included: voxel size = 14×14×14 mm (volume =2.744 cm3), TE = 35 ms; TR = 2 s for a total acquisition time of ~3 min. MRS voxels were placed according to several strategies described below.

2.3. Identification of rs-fMRI cluster for guided voxel prescription

While both structural and functional targets are compatible with our automated MRS voxel placement procedure, here we investigated the reliability and utility of MRS targets that were defined functionally given previous methods have validated the utility of structurally defined approaches using atlas based coordinates.

In both studies, resting state functional connectivity clusters were identified to guide clinical TMS therapy for either chronic pain (Study A) or depression (Study B) providing a relevant paradigm for future application of this automated voxel prescription technique. In Study A, a voxelwise analysis of the rs-fMRI scan was analyzed to determine the subregion of the L-DLPFC (Brodmann Area 9 + 46) that exhibited the greatest correlation with the dorsal anterior cingulate (dACC) (Faerman et al., 2021). In Study B, a voxelwise analysis of the rs-fMRI scan was analyzed to determine the subregion of the L-DLPFC (Brodmann Area 46) exhibiting the greatest anti-correlation to the subgenual cingulate

(sgCC) (Cole et al., 2020).

2.4. Voxel prescription procedures

In the two studies we implemented three voxel prescription approaches: 1) manual, 2) semi-automated, and 3) automated. Each of the study specific protocols are outlined in detail below and typically can be completed concurrently during other desired acquisitions (i.e., structural or additional spectroscopic acquisitions, etc.) in several minutes or less:

In Study A, semi-automated and automated approaches were used. The baseline resting state fMRI scan (from the MRI #1; Fig. 2) was first analyzed as described above. On the subsequent independent pre- and post-TMS MRI sessions, L-DLPFC Optimized-PRESS and MEGA-PRESS voxel prescription was performed using two different iterations of our voxel prescription procedure termed semi-automated and an automated based on amount of required user input and fine tuning. For both prescription approaches, the center of gravity coordinate (mm) of the identified L-DLPFC functional cluster was extracted using the FSL Software (Version 6.0) via the fslstats function with the lowercase "c" flag (e.g. fslstats fmri_cluster.nii -c). In the semi-automated voxel placement approach, participants then underwent a pre-TMS MRI. During this imaging session, a T1w image was collected prior to either MEGA-PRESS, Optimized-PRESS, or both. Immediately following completion of the T1w image acquisition, a custom script was used to pull the MRI data directly from the imaging server. The T1w image was then reconstructed into Neuroimaging Informatics Technology Initiative (NIFTI) format. Next, a second in-house MATrix LABoratory (MATLAB; R2015a, The Mathworks, Inc.) script utilizing Statistical Parametric Mapping software version 12 functions (SPM12; Wellcome Trust Centre for Neuroimaging). The baseline (MRI #1) T1w and pre-TMS (MRI #2) T1w images were co-registered while the participant underwent additional study specific MRI acquisitions. Co-registration was achieved using the spm_coreg.m function. Affine transformation matrices were defined using an optimized normalized mutual information approach (Collignon et al., 1995; Colin et al., 1998; Press et al., 1992). Resulting affine transformation matrices were then used to convert the fMRI-based L-DLPFC center-of-gravity coordinate from baseline (MRI #1) to pre-TMS MRI space.

Pre-TMS MRI voxel prescription for both Optimized-PRESS and MEGA-PRESS was then setup in two steps. First, voxel rotations were manually aligned to the skull geometry in the sagittal plane using a shim acquisition. Once the appropriate rotation was achieved and copied to either the MEGA-PRESS or Optimized-PRESS sequence, the voxel size was specified (MEGA-PRESS = 20×20×20 mm and Optimized-PRESS 14×14×14 mm) and the co-registration-defined coordinate (described above) was then input into the scanner console interface. This resulted in the placement of the center of the MRS voxel at the center of the desired functional ROI (Fig. 2). The term semi-automated pipeline was used due to the superficial nature of the cortical targets which required manually translating the voxel to ensure only brain tissue was encompassed within the bounding box (i.e., not skull and other non-brain tissue that can influence the MRS measurement). For the semi-automated pipeline group, this process, with the slight manual translation, was then repeated for all subsequent MRI sessions (Fig. 2**D top**).

To further remove the required translation step from all but the first MRS acquisition, an automated procedure was developed. This automated method first implements the semi-automated approach as described above for registration from MRI #1 to MRI #2, followed by an increasingly automated procedure that removes the tuning step initially required to translate the MRS voxel to avoid non-brain tissue. This is achieved by directly co-registering the translated MRS center of gravity coordinate from MRI #2 for all subsequent acquisitions. The output of this procedure is thus a new co-registered coordinate that does not require additional manual adjustment for any subsequent repeated acquisition (Fig. 2).

In Study B, MRS (MEGA-PRESS only) scans were acquired at baseline (MRI #1), after one week, and again after one month (Fig. 2) using manual or semi-automated voxel prescription approaches. Voxel prescription at baseline was conducted manually according to neuroanatomy without the use of any semi- or automated voxel placement procedures. In brief, the voxel was aligned to the angle of the skull in the sagittal plane. Co-registration of the Brodmann Area 46 mask in standard space to the subjects T1-weighted image was first conducted and then the voxel was manually transcribed to center of the mask by visualizing participant specific anatomical landmarks. The 1-week and 1-month voxels were prescribed using the semi-automated approach described above. (Fig. 2).

2.5. Voxel composition

GM and WM voxel segmentation fractions were evaluated across prescription protocols to determine the consistency and reliability of semi-automated and automated approaches. Both Freesurfer and the SPM segmentation output which is standard in the Gannet MRS processing package were assessed.

Freesurfer Analysis: T1w images were segmented using Freesurfer software (Version 6; (Fischl et al., 2002)). Next, a custom MATLAB script was utilized to extract the 3-dimensional (3D) voxel mask from the raw MRS data (i.e., GE p-file). The scanner-reconstructed T1w image was then reoriented to standard space (fslreorient2std; FSL software toolbox) and the 3D voxel mask and script-generated T1w image geometries were standardized using the flscpgeom command. AFNI (Cox, 1996) 3dcalc was then used to compute the WM, GM, and cerebrospinal fluid (CSF) segmentation percentages of the 3D voxel from the Freesurfer generated segmentation (aseg.mgz) file.

SPM Analysis: The Gannet Software toolbox (Edden et al., 2014) is a freely available software suite that is commonly used to process and analyze MEGA-PRESS data. Gannet processing includes the option to implement batch tissue segmentation using SPM12 Software (Ashburner and Friston, 2005). GM, WM, and CSF tissue fractions were extracted from the MEGA-PRESS p-files using SPM via the GannetSegment function in the Gannet software toolbox (Version 3.0). Subsequent statistical analyses were carried out on GM and WM tissue fractions.

Although it is not within the scope of this manuscript to directly compare tissue segmentation approaches (i.e., Freesurfer vs. SPM), tissue fraction differences within the MRS voxel are known to influence metabolic concentration (Porges et al., 2017; Harris et al., 2015). For this reason, both Freesurfer and SPM segmentations were generated and compared.

2.6. Spatial consistency of voxel placement

2.6.1. Euclidean distance analyses

Euclidean distance from the center-of-gravity voxel coordinates across MRI timepoints were calculated to evaluate the stability of each of the prescription protocols (i.e., Study A MEGA-PRESS semi-automated vs. automated; Study A Optimized-PRESS semi-automated vs. automated; Study B MEGA-PRESS manual vs. semi-automated). Distance analyses were conducted in subject (T1w) space using FSL Software. For both Study A and Study B protocols, subjects' T1w scans for all MRI timepoints (MRI #2 and MRI #3) were linearly registered (flirt) to the baseline MRI (MRI #1) for both Study A and Study B. Next, the MRS voxels for each subsequent timepoint were co-registered to the baseline MRI scan. Three-dimensional center-of-gravity coordinates (mm-space) were extracted for each voxel and Euclidian distance was calculated.

2.6.2. Dice similarity coefficient

To examine the spatial overlap of the MRS voxels, the Sørensen–Dice Similarity Coefficient (DSC) was implemented (SØRensen, 1948; Dice, 1945). This is also referred to as the dice overlap coefficient. Each subjects T1w scans were co-registered to their baseline T1w scan using

FSL LInear Registration Tools (FLIRT) with no resampling of the MRS voxels. DSC was then calculated in RStudio (*RStudio Team (2020). RStudio: Integrated Development for R. RStudio, PBC, Boston, MA URL http://www.rstudio.com/)* with the FSL wrapper functions (https://rdrr.io/cran/fslr/man/fsl_dice.html). DSC was computed across all pipelines using binarized pre- and post- MRS voxel masks which are represented in the equation below as A and B respectively. DSC outputs range from 0, representing no overlap, to 1 which represents complete overlap.

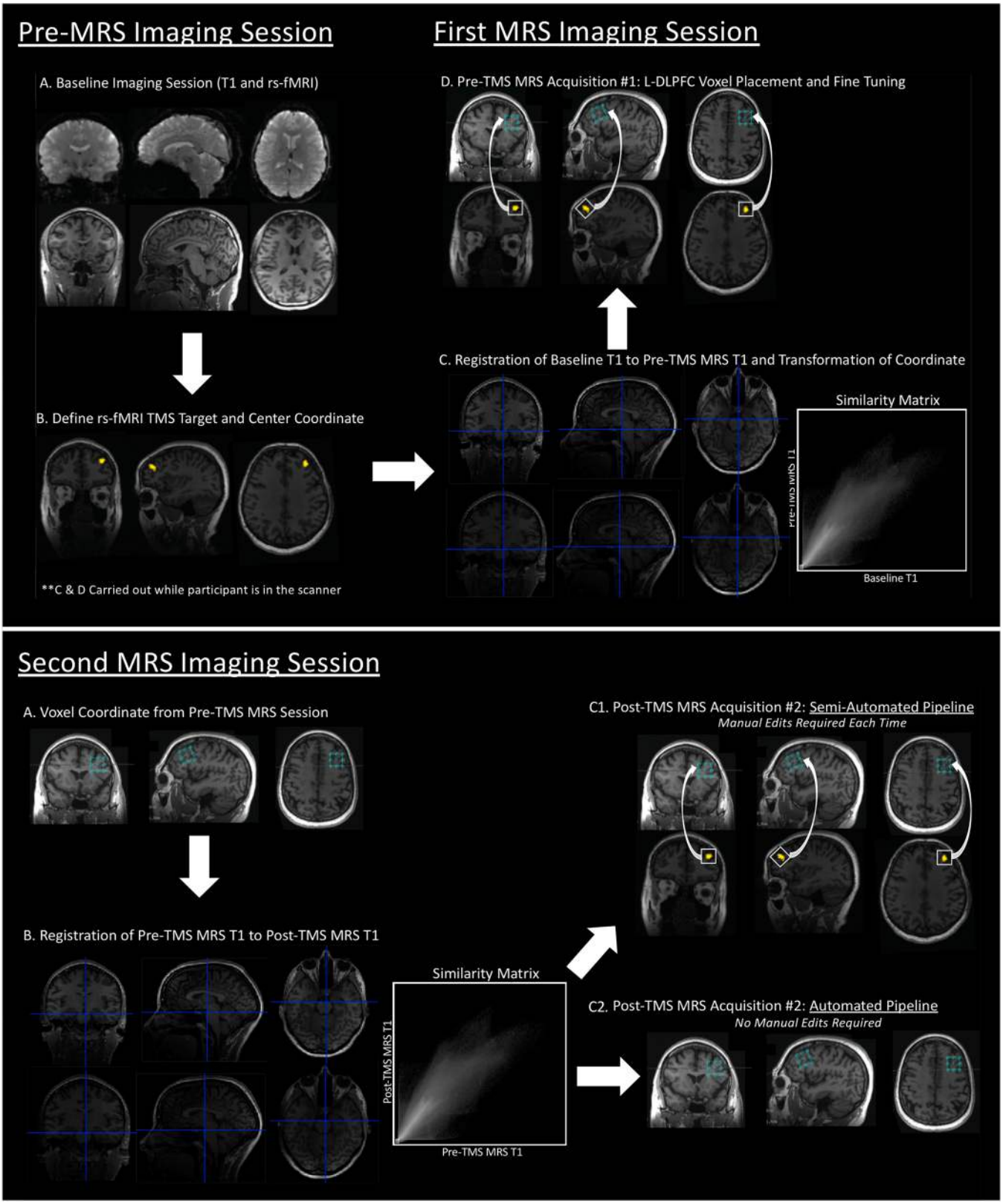

(caption on next page)

Fig. 2. VOI Prescription Schematic: Schematic of semi-automated and automated voxel prescription procedure (standard manual voxel prescription conducted during the initial, "Pre-MRS", imaging session of Study Bl not shown). Top A) Pre-MRS Imaging Session: An MRI session consisting of T1w and resting state acquisitions (Study A) and also a manually prescribed L-DLPFC MEGA-PRESS scan for Study B. Top B) Resting state images from pre-MRS imaging session were preprocessed and analyzed to define a functional ROI within the L-DLPFC. The center-of-gravity coordinate for the functional cluster was then determined using FSL tools (fslstats). Top C) During the second imaging session (MRS-Session 1 Study A; and 2 for Study B), a T1w was first acquired. Upon completion of the scan, the T1w image was pulled directly from the MR system server, reconstructed, and co-registered to the pre-MRS T1w image. Top D) MRS voxel rotation aligned with the slope of the skull in the sagittal plane and the co-registered center-of-gravity coordinate in the current subject space was input into the scanner. Voxel location adjustments were made to ensure the entirety of the voxel was within brain tissue and did not encompass meninges or skull. Following minor adjustments, the final center-of-gravity voxel coordinates were documented from the scanner console for use in the subsequent independent MRS sessions (Bottom A). These coordinates could also be obtained using FSL software. The described procedure requires several minutes to complete (< 3 in our experience). Second MRS Imaging Session: For the semi-automated voxel prescription pipeline the identical procedure described above was repeated (Bottom B and C1). For the automated voxel prescription pipeline, the T1w image was again acquired first, directly pulled from the MR system server, and reconstructed (Bottom B). This time the current T1w image was co-registered to the first MRS T1w image along with the documented center-of-gravity coordinate defined after adjustments were made (Bottom C2). Voxel rotation was aligned with the slope of the skull in the sagittal plane and the computed coordinate was input into the scanner software. If done correctly no further manual modification to the voxel location was required.

Greater overlap indicates greater consistency across the multi-session data.

$$DSC = \frac{2(A \cap B)}{A + B}$$

2.7. Statistical analyses

All statistical analyses were carried out in RStudio (Version 2018 1.2.1335). To determine the appropriate downstream statistical test to investigate differences in variability (SD) and means (M), both homogeneity of variance and normality were first assessed for segmentations (GM and WM), Euclidean distance, and overlap coefficient variables. Normality (distribution) of each variable was evaluated using the Shapiro-Wilk normality test (Shapiro and Wilk, 1965). Homogeneity of variances were assessed between groups using either a standard *F* test if the variable(s) were normally distributed or alternatively with the non-parametric Fligner-Killeen Test (Conover and Iman, 1981) if there

Table 1
Voxel Composition Across Multi-Acquisition and Longitudinal Studies: Tissue fraction statistics for each project across voxel prescription approaches, MRS acquisitions of different sizes, and segmentation methods. Statistically significant differences are indicated by (*). Non-parametric tests were used when data was not normally distributed. (GM=Grey Matter; WM=White Matter; M=Mean; SD=Standard Deviation).

Study A – Δ Freesurfer Segmentation – MEGA-PRESS (20x20x20mm)									
		GM				**WM**			
Voxel Prescription	**N**	**M**		**SD**		**M**		**SD**	
Semi-Automated	26	-0.00209		0.0462		0.00373		0.0654	
Automated	24	-0.00466		0.0119		0.00451		0.0127	
		χ^2	**t [95% CI]**	**df**	**p**	χ^2	**t [95% CI]**	**df**	**p**
T-test		-	-0.27 [-0.02, 0.02]	28.54	0.79	-	0.06 [-0.03, 0.03]	27.03	0.95
F-test		16.04	-	1	6.20^{-05}*	14.84	-	1	0.000117*
Study A – Δ SPM Segmentation – MEGA-PRESS (20x20x20mm)									
		GM				**WM**			
Voxel Prescription	**N**	**M**		**SD**		**M**		**SD**	
Semi-Automated	26	0.00358		0.0373		-0.00854		0.054	
Automated	24	0.000458		0.0180		0.00338		0.0196	
		χ^2	**t [95% CI]**	**df**	**p**	**F**	**t [95% CI]**	**df**	**p**
T-test		-	-0.37 [-0.02, 0.01]	33.17	0.71	-	1.02 [-0.01, 0.04]	28.96	0.318
F-test		6.03	-	1	0.01*	0.13	-	[23, 23]	7.67^{-06}*
Study A – Δ Freesurfer Segmentation – Optimized-PRESS (14x14x14mm)									
		GM				**WM**			
Voxel Prescription	**N**	**M**		**SD**		**M**		**SD**	
Semi-Automated	18	-0.0146		0.0458		-0.00412		0.0394	
Automated	31	-0.00737		0.0341		-0.000291		0.0318	
		χ^2	**t [95% CI]**	**df**	**p**	χ^2	**t [95% CI]**	**df**	**p**
T-test		-	0.60 [-0.02, 0.03]	30.21	0.55	-	0.36 [-0.02, 0.03]	32.16	0.72
F-test		0.60	-	1	0.44	0.39	-	1	0.53
Study B – Δ Freesurfer Segmentation – MEGA-PRESS (20x20x20mm)									
		GM				**WM**			
Voxel Prescription	**N**	**M**		**SD**		**M**		**SD**	
Manual	20	0.00998		0.0898		-0.00696		0.142	
Semi-Automated	18	-0.00453		0.0457		0.00417		0.0472	
		F	**t [95% CI]**	**df**	**p**	**F**	**t [95% CI]**	**df**	**p**
T-test		-	-0.64 [-0.06, 0.03]	28.82	0.53	-	0.33 [-0.06, 0.08]	23.54	0.74
F-test		0.26	-	[17, 19]	0.007*	0.11	-	[17, 19]	3.08^{-5}*
Study B – Δ SPM Segmentation – MEGA-PRESS (20x20x20mm)									
		GM				**WM**			
Voxel Prescription	**N**	**M**		**SD**		**M**		**SD**	
Manual	20	0.00220		0.0908		-0.0008		0.123	
Semi-Automated	18	-0.00439		0.0413		0.00356		0.0500	
		F	**t [95% CI]**	**df**	**p**	**F**	**t [95% CI]**	**df**	**p**
T-test		-	-0.29 [-0.05, 0.04]	27.14	0.77	-	0.15 [-0.06, 0.07]	25.68	0.89
F-test		0.21	-	[17, 19]	1.97^{-3}*	0.17	-	[17, 19]	4.97^{-4}*

was a significant deviation from normality ($p < 0.5$). Between group mean differences were determined using unpaired two-sample *t*-tests. If data were not normally distributed a Wilcoxon non-parametric test was implemented.

3. Results

3.1. Voxel composition

GM and WM composition of the L-DLPFC VOIs was assessed by first calculating the difference in longitudinal tissue fraction (Post-Pre) across prescription pipelines using standard segmentation approaches including both Freesurfer and SPM (Table 1 **&** Fig. 3). In Study A (MEGA-PRESS: $N = 50$; semi-automated = 26, automated = 24; Optimized-PRESS: $N = 50$; semi-automated = 18, automated = 31), individuals underwent longitudinal MRI scanning approximately one-hour apart and semi-automated voxel prescription was compared to automated voxel prescription. Three participants in each of Study A and Study B were excluded from the analyses due to poor data quality and/or registration related issues (e.g., scanner related shim error). No significant between-pipeline differences in GM or WM voxel composition were identified for either MEGA-PRESS (voxel size = 20×20×20mm) or Optimized-PRESS acquisitions (voxel size = 14×14×14mm) across segmentation methods. A significant between-pipeline difference in variance was observed in the MEGA-PRESS acquisition for both Freesurfer and SPM segmentations (Table 1), demonstrating a reduction in variability in voxel composition of both GM and WM with the automated prescription approach. Alternatively, tissue composition of the smaller Optimized-PRESS acquisition did not yield significant between-pipeline differences in either mean or variance.

In Study B (N = 38; manual=20, semi-automated=18), individuals underwent longitudinal MRI scanning at three independent timepoints: baseline, one-week, and one-month. Manual prescription occurred at baseline and semi-automated functional connectivity guided placement occurred at one-week and 1-month utilizing the same functional-connectivity derived coordinate. Similar to Study A, the mean GM and WM fractions were not significantly different between voxel placement pipelines for either segmentation approach (Fig. 3). Also consistent with Study A, a significant between-pipeline difference in variance was identified across voxel prescription pipelines and segmentation approaches (Table 1 **&** Fig. 3).

Spatial congruency of the repeated MRS voxel prescriptions was also assessed by computing a dice similarity coefficient DSC). Analyses were completed in individual subject space (T1w image-space) without the need for resampling the MRS voxel. Outputs of the DSC range from 0 (no overlap) to 1 (complete overlap). Representative prescribed MRS voxels utilizing semi-automated and automated techniques for both MEGA-PRESS and Optimized-PRESS acquisitions are demonstrated in 3D by the Cyan and red cubes (Top). The table below illustrates that the more automated the voxel prescription procedure the more spatial overlap regardless of voxel size. This is consistent in Study A where independent scans were acquired an hour apart and the automated pipeline outperformed the semi-automated prescription procedure with regard to overlap of the repeated placement. In Study B, the semi-automated prescription procedure outperformed the manual placement procedure even with increased duration between scans in the automated data acquisition, that is: Manual prescription data were acquired one-week apart and semi-automated data were acquired 1-month apart. (N = number of participants; M = mean; SD = Standard Deviation).

3.2. Spatial consistency: euclidean distance & DSC

DSC was computed and compared to further characterize the extent of spatial overlap between voxel prescription pipelines (Fig. 4.). Euclidean distance was calculated and compared across acquisitions to assess the movement of the center-of-gravity for the MRS voxel (Fig. 5). Three participants in each of Study A and Study B were excluded from the analyses due to poor data quality and/or registration related issues (e.g., scanner related shim error). In Study A, the automated voxel prescription performed significantly better than semi-automated placement for both MEGA-PRESS and Optimized-PRESS acquisitions as indicated by increased spatial overlap across repeated scans and a reduction in center-of-gravity Euclidean distance. This was demonstrated by large effect sizes across statistical comparisons of both DSC and Euclidian distance: MEGA-PRESS DSC (Cohen's d = 1.75, 95% CI = [1.09, 2.40]), MEGA-PRESS Euclidean distance (Cohen's d = −1.76, 95% CI = [−2.41, −1.10]), Optimized-PRESS DSC (Cohen's d = 1.38, 95% CI = [0.94, 1.82]), and Optimized-PRESS Euclidean distance (Cohen's d = −1.59, 95% CI = [−2.04, −1.13]),. Similarly, in Study B, semi-automated voxel prescription significantly outperformed manual placement in both spatial overlap (DSC) of the voxels and center-of-gravity Euclidean distance even with the increased duration between scans, that is: one-month vs. one-week. Effect sizes were also respectively large: MEGA-PRESS DSC (Cohen's d = 2.42, 95% CI = [1.52, 3.29]) and MEGA-PRESS Euclidean distance (Cohen's d = −2.25, 95% CI = [−3.10, −1.38]). To examine potential voxel warping effects on DSC, the post registered voxel sizes for both MEGA-PRESS and NFL-PRESS were evaluated for Study A. Non-parametric t-tests were performed because the data were not normally distributed. The average MEGA-PRESS voxel volume for the pre (Automated: M=8016, SD=184; Semi-Automated: M=7980, SD=179) and post (Automated: M=7999, SD=148; Semi-Automated: M=8009, Standard D=183) coregistered MRS voxels between groups were not statistically significant: pre ($z = -0.57$, $p = 0.56$) and post ($z = -0.84$, $p = 0.40$) respectively. (M=Mean; SD=Standard Deviation).

4. Discussion

Here we report on novel voxel prescription pipelines that enable increasingly robust voxel prescription for multi-acquisition as well as longitudinal MRS applications. To evaluate the consistency of these approaches across several iterations of varying automation, we investigated the spatial and anatomical reproducibility of repeated MRS acquisition across two independent datasets. Validation of the technique was performed quantitatively by examining the change in Euclidean distance of the voxel center-of-gravity, defining the overlap of voxels using the DSC, and by evaluating the voxel tissue composition fraction across acquisitions. Results of both datasets are consistent, demonstrating less variance across repeated prescriptions with increasing automation of the prescription approach - even in data acquired over a broad timeframe (i.e., one month between MRS acquisitions).

As personalized clinical interventions continue to gain traction, parallel improvements in methods used to measure clinical changes are necessary to identify underlying pathology and/or evaluate treatment course. Ultimately, the choice of acquisition method may depend on the research question at hand and particularly whether effects are expected to be focal or widespread. For example, it could be reasonably hypothesized that systemic pharmacological interventions exert brain-wide effects and thus automation of voxel prescription may not be warranted. Alternatively, the use of imaging acquisitions or modalities (i.e., functional, structural, positron emission tomography) to guide voxel placement would not only be useful for placement but also to provide biological or physiological justification for positioning within a structure. On the other hand, for investigations utilizing targeted neuromodulation paradigms such as transcranial magnetic stimulation, focused ultrasound, or focal drug release methods, the use of automated techniques that are not solely based on anatomical landmarks is critical.

In both studies, automated and semi-automated center-of-gravity Euclidean distance and DSC demonstrated highly reproducible voxel placements. While consistent manual voxel prescription has been reported in brain regions with well-defined boundaries and/or structural features (Bai et al., 2017), it is worth noting that the DLPFC results

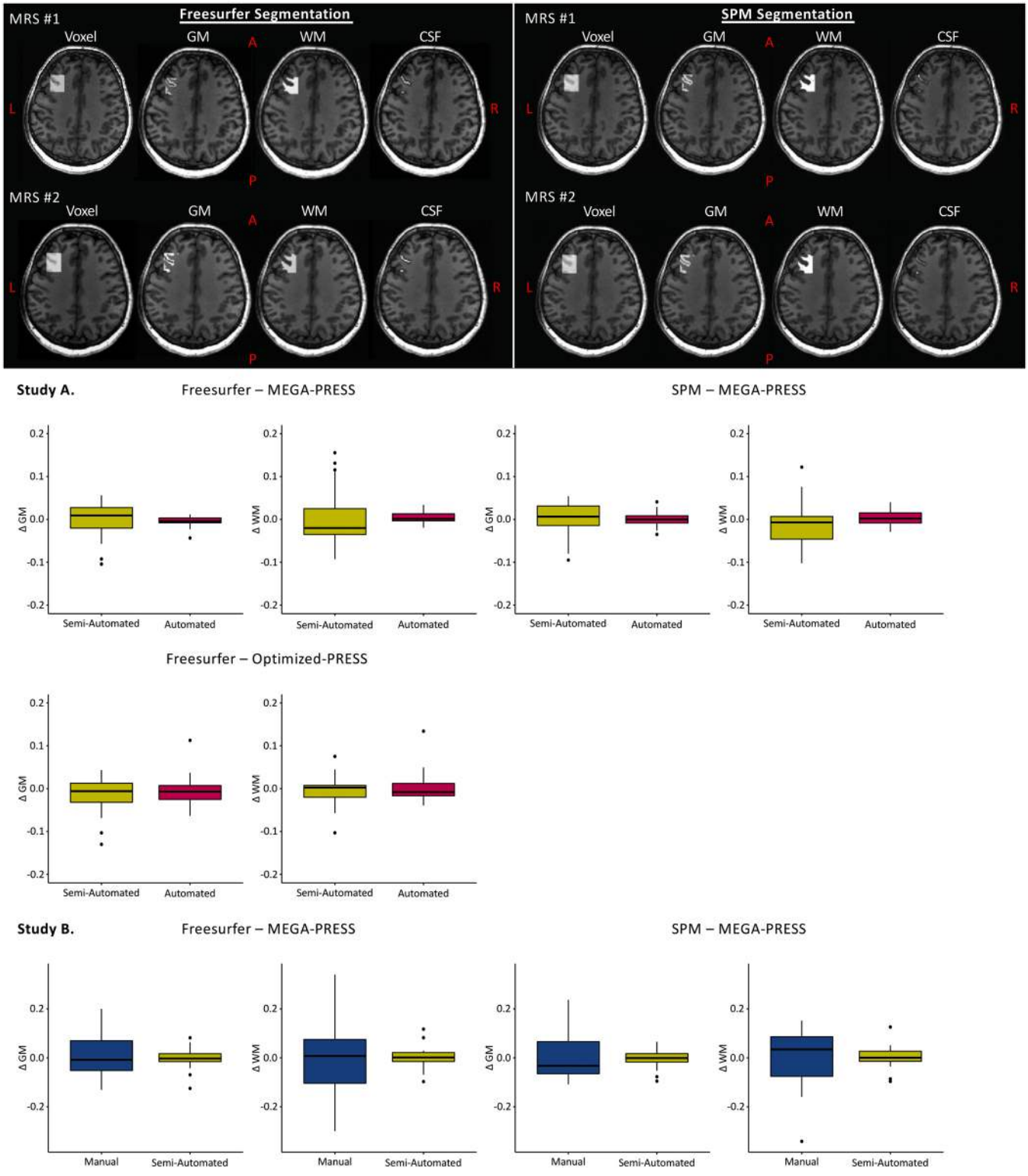

Fig. 3. Multi-Acquisition / Longitudinal L-DLPFC Voxel Tissue Composition: Tissue fractions were determined by calculating the differences between Freesurfer and SPM segmentations across repeated independent MEGA-PRESS and Optimized-PRESS acquisitions of difference voxel sizes. In Study A, tissue delta was defined as Post MRI – Pre MRI GM and WM tissue fractions for both semi-automated and automated prescription pipelines (Top). Study B included only MEGA-PRESS acquisitions, with identical scan parameters as Study A. GM and WM tissue fractions for manual and semi-automated placement were determined by computing the difference between the one-week MRI – baseline MRI and one-month MRI – one-week MRI respectively. With the exception of the Study A Optimized-PRESS measures, the more automated prescription procedures reduced variability of tissue fraction.

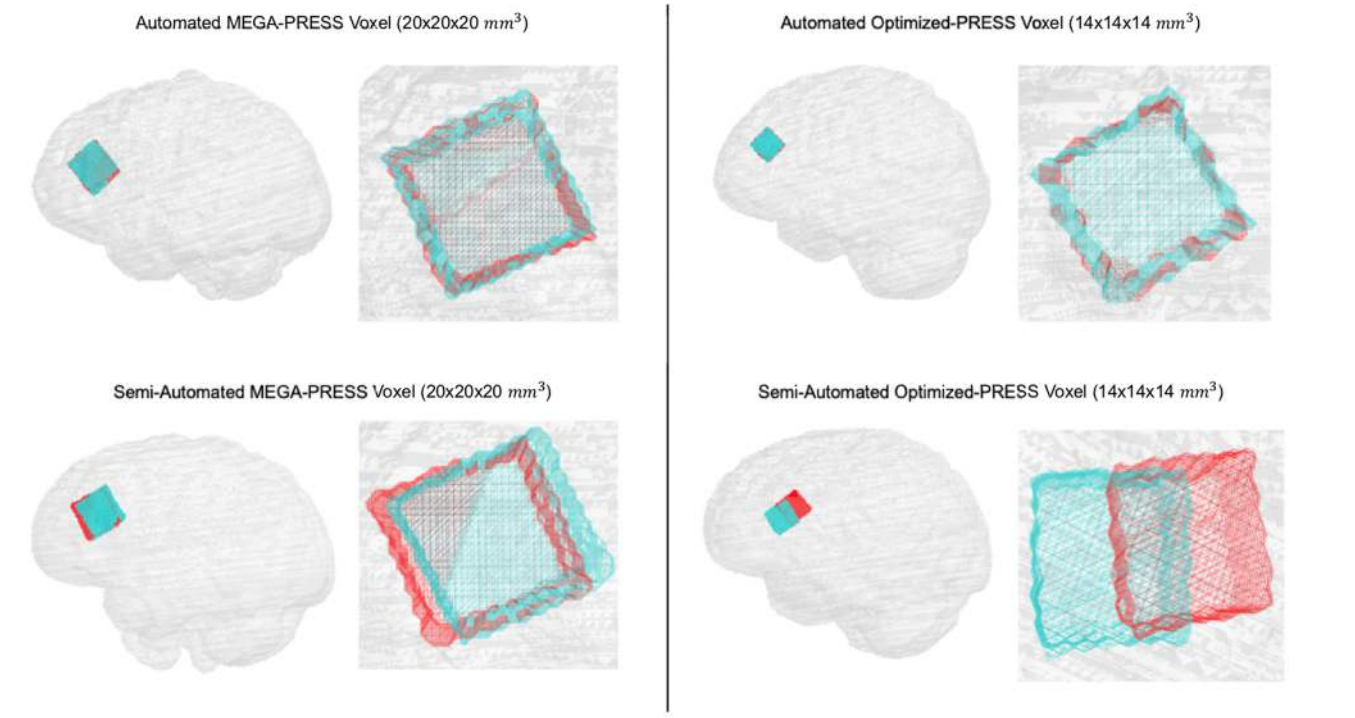

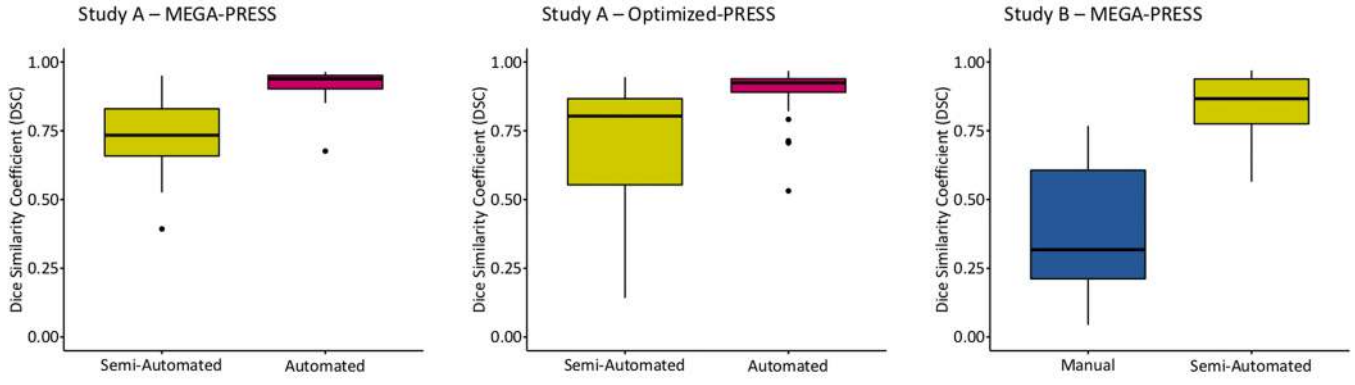

	Study A - MEGA-PRESS					Study A - Optimized-PRESS						Study B - MEGA-PRESS				
Voxel Prescription	**N**	**M**			**SD**	**N**	**M**			**SD**	**Voxel Prescription**	**N**	**M**			**SD**
Semi-Automated	26	0.731			0.138	19	0.688			0.235	**Manual**	19	0.392			0.232
Automated	24	0.921			0.060	31	0.891			0.092	**Semi-Automated**	16	0.846			0.115
	χ^2	t	[95% CI]	df	p	χ^2	t	[95% CI]	df	p		χ^2	t	t [95% CI]	df	p
T-test	-	6.37	[0.13, 0.25]	34.67	2.66_{-7}*	-	3.60	[0.09, 0.32]	21.46	0.001649*	**T-test**	-	7.51	[0.33, 0.58]	27.28	4.17_{-8}*
F-test	11.55	-	-	1	0.0006775*	12.47	-	-	1	0.0004127*	**F-test**	5.62	-	-	1	0.01776*

Fig. 4. L-DLPFC VOI Spatial Overlap.

demonstrated here were observed using relatively small VOIs in the absence of a specific set of anatomical landmarks. This further underscores the utility of our approach for functionally defined regions-of-interest. In developing the voxel placement procedure, two versions of the pipeline were created, referred to as semi-automated and automated. These approaches are similar with the addition of one adjustment step at the end. This adjustment step is critical for MRS collected in superficial brain structures such as the cortex or immediately adjacent to a sinus to ensure that voxels are completely bound to brain tissue. In deep brain structures this adjustment step would likely not be necessary. Although neither study directly compared all three approaches (manual, semi-automated, and automated) head-to-head, we demonstrated that increased automation of the voxel prescription process achieves highly spatially consistent voxels with marked reductions in within-subject tissue fraction variability. The distance and spatial overlap analyses provide complementary data that

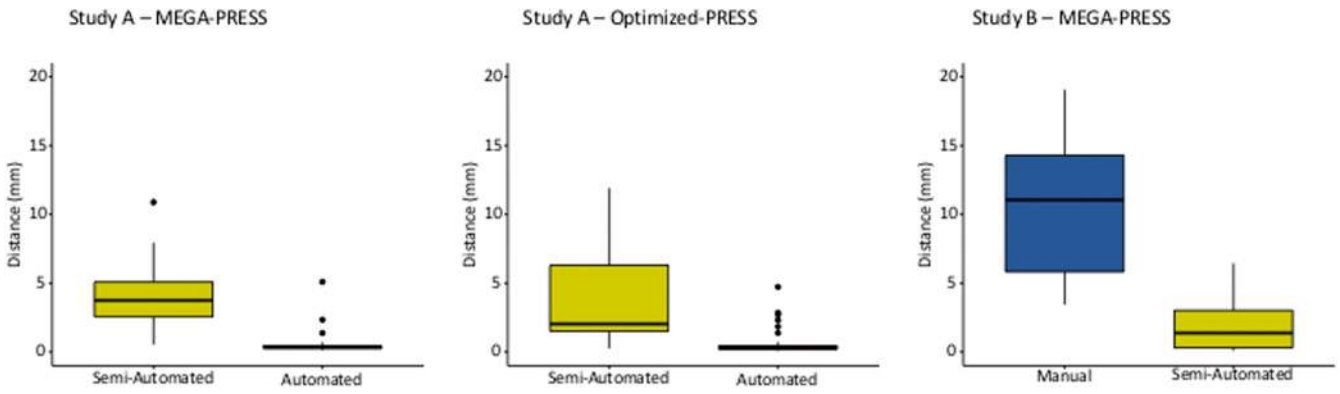

	Study A - MEGA-PRESS				Study A - Optimized-PRESS					Study B - MEGA-PRESS				
Voxel Prescription	N	M	SD		N	M	SD		Voxel Prescription	N	M	SD		
Semi-Automated	26	3.98	2.41		19	4.19	3.55		Manual	19	10.60	4.89		
Automated	24	0.66	1.06		31	0.74	1.07		Semi-Automated	16	1.95	1.94		
	χ^2	t [95% CI]	df	p	χ^2	t [95% CI]	df	p		χ^2	t [95% CI]	df	p	
T-test	-	-6.40 [-5.29, -1.93]	34.87	2.33^{-07}*	-	-4.13 [-5.20, -1.71]	20.01	0.0005218*	T-test	-	-7.07 [-11.16, -6.12]	24.32	2.44^{-07}*	
F-test	17.40	-	1	3.02^{-05}*	15.40	-	1	8.70^{-05}*	F-test	8.33	-	1	0.003891*	

Fig. 5. L-DLPFC Multi-Acquisition / Longitudinal Euclidean Distance: Automated voxel placement reduced variability and mean distance of center-of-gravity measurements. To determine the amount of change in geometric centers of prescriptions following repeated acquisitions, center-of-gravity coordinates were extracted for each voxel and Euclidean distance was calculated. Automated approaches reduced distance measurements across both MRS acquisition size and study cohorts (N = number of participants; M = mean; SD = Standard Deviation).

provide empirical evidence in support of this conclusion. Both the mean and variability of the distance measurements in the semi-automated pipeline did not increase across studies, even with increased time between scans (i.e., 1-month vs. 1-hour), and thus demonstrate the utility of this method across multi-acquisition and longitudinal study designs.

A source of variability not specifically accounted for in the outlined automation approaches is voxel rotation and is an area that warrants ongoing methodological development. To overcome this the present studies, the slope of the skull in the sagittal plane was used to guide voxel rotation, however, users will need to establish a set of criteria for consistent voxel rotation. The proposed voxel-placement methods do not completely obviate this challenge and source of variability from manual input particularly for subcortical VOIs. While the Euclidean distance comparison does not account for this potential source of variability as it is based on voxel center of gravity, the DSC does. This is because DSC determines the overlap of two volumes (here binary masks) that is thus useful for determining the effects that inconsistencies in rotation may have on the prescription pipeline. Our DSC results are consistent with a previously reported automated voxel prescription method that guides voxel placement based on anatomical ROIs (Park et al., 2018), however, in the latter approach resampling is required. Resampling necessitates a modified calculation of the overlap coefficient that is termed the *generalized dice coefficient*. Additionally, Bai and colleagues assessed the reproducibility of manual voxel prescription by prescribing and acquiring the MRS voxel multiple times within a single scan session (i.e. patients were not removed from the scanner between acquisitions; (Bai et al., 2017)). Here we demonstrate that the spatial consistency of the automated and semi-automated approaches across multiple imaging sessions yielded greater inter-subject overlap coefficients comparatively even given the potential variability introduced by non-automated voxel rotation.

Consistency in data collection is critical for methodologies used in any research application and if not it begs to question the validity of the measurement. MRS is currently one of the only non-invasive imaging techniques that can measure neurochemical concentrations in vivo. Reducing unwanted sources of variability during MRS voxel prescription will lead to more consistent and meaningful results in human neuroscience, particularly when focal interventions are being evaluated. For example, as metabolic molecule concentrations vary across tissue type (Porges et al., 2017; Harris et al., 2015), tissue concentration within the MRS voxel influences the acquired measurements (Gasparovic et al., 2006). For example glutamate and glutamine concentrations have been shown to be higher in concentration within GM compared to WM (Hurd et al., 2004) highlighting the advantage of reduced GM and WM tissue fraction variability observed using automated voxel placement approaches. Collectively, these findings strengthen the utility of MRS applications to examine multi-session/longitudinal MRS data, in relation to basic and clinical research questions including effects of interventions. Future investigation is warranted to determine whether the automated approaches adapted for single-session MRS reduce MRS tissue fraction variability. Alternatively, voxel placement grounded on biological or physiological data rather than standardized anatomical guidance, may provide a more useful study measure, even if it increases between-subject spatial variability in voxel location. Although the data presented demonstrates longitudinal consistency within-subjects using individualized fMRI coordinates, the described approach is methodologically adaptable for between-subject designs using either structural or functional coordinates from a standard brain atlas, literature coordinate, or meta analysis.

Finally, reproducibility in neuroimaging is critical for both research and clinical applications. MRS is particularly susceptible to scrutiny on this front using standard voxel prescription methods that are dependent on user expertise. Automated pipelines, such as those described here, promise to broaden the applicability and generalizability of MRS. This is especially applicable for large-scale multi-center trials and investigations that are becoming increasingly common. In the current

study, independent research staff without expertise in neuroanatomy acquired both independent datasets. The consistency of results among multiple users is strong evidence of the methods ease of use and demonstrates the applicability to standardize voxel placement across laboratories and institutions.

4.1. Caveats

The current study evaluated the utility of using pre-determined functional ROIs generated from previous independent imaging sessions to guide the automated placement of MRS voxels. This requires an established analysis protocol that can be completed in a relatively short timeframe prior to follow-up imaging session. This may not be practical for all investigative teams. Real-time resting state analysis methods would enable the acquisition and analysis of functional imaging paradigms during the same session, and while frequency drift has been noted as a major concern for running gradient intensive sequences prior to collecting MRS, recent largescale data suggest that few scanners exhibit moderate to severe drift following fMRI using echo planar imaging (Hui et al., 2021). Alternatively, the automated approaches proposed in this manuscript could be easily adapted to perform multi-acquisition and longitudinal placement using coordinates from standardized brain coordinates (structural or functional) as well as structural ROIs following manual placement, although not formally tested in this manuscript. That is, manual prescription could be implemented initially, and the center-of-gravity coordinate of the MRS voxel could be documented and input into the co-registration steps for subsequent scans to achieve consistency of placement across repeated acquisitions.

Another caveat not addressed in this manuscript is the ease of adapting this method across MRI vendors and imaging facilities. While the majority of steps are performed using an independent laptop or scanner computer with access to Matlab, FSL, and SPM, variability in vendor software may require adaptation of the current approach. We also acknowledge that this investigation does not provide direct comparison to other available voxel prescription methods and thus no interpretation can be made as to the superiority of one method versus another. Until direct comparisons are made, user preference may ultimately be decided by ease of use, study design, or research question.

Finally, the methods used to evaluate voxel prescriptions are not without limitations. Registration can cause warping of the voxel which could influence overlap outcomes. Evaluation of these effects demonstrated little deviation from expected voxel volumes and differences between pipelines were not statistically significant.

4.2. Summary and conclusions

Our results provide evidence for the reliability and reproducibility of two pipelines that enable real-time automated MRS voxel prescription over multi-acquisition and longitudinal experimental approaches. The complementary analyses and associated results highlight the utility of our approaches compared to manual procedures, that is: (Stanley and Raz, 2018) greater consistency of tissue fraction within MRS voxels; (Schur et al., 2016) the reduction of distance between center-of-gravity measurements; and (Oz et al., 2020) substantial overlap as measured by the DSC across multiple users and projects. Together these results suggest that our approach provides a meaningful step toward the standardization of MRS data acquisition that is relevant for a variety of MRS research designs that consist of multiple users and laboratories. Our approach reduces the reliance on technician expertise during MRS data acquisition by standardizing voxel prescription and thus broadens the usability and feasibility of MRS as an investigative tool in neuroscience.

Funding

This work was supported by the NIH National Center for Complementary and Integrative Health grants 5R33AT009305–03 (NW & DS), 1F32AT010420–01 (JB), The Stanford University Molecular Imaging Scholars Fellowship (T32CA118681; JB), and the Center for Neurobiological Imaging Innovation Award (JB). MDS and the Meditation Research Program are supported by the National Institute of Mental Health (Project Number R01MH125850), Dimension Giving Fund, Ad Astra Chandaria Foundation, Brain and Behavior Research Foundation (Grant Number 28972), BIAL Foundation (Grant Number 099/2020), Emergence Benefactors, The Ride for Mental Health, and Gatto Foundation. Additional data were provided by the Brain Stimulation Laboratory directed by (NW) and supported by Charles R. Schwab, the Gordie Brookstone Fund, the Marshall & Dee Ann Payne Fund, the Avy L. and Robert L. Miller Foundation, a Stanford Psychiatry Chairman's Small Grant, NARSAD Young Investigator Award, and the Stanford Department of Psychiatry and Behavioral Science.

CRediT authorship contribution statement

Conceptualization: **James H. Bishop**, **Matthew D. Sacchet;** Data curation: **James H. Bishop**, **Naushaba Khan**, **Claudia Tischler**, **Ruben Krueger**; Formal analysis: **James H. Bishop**; Funding acquisition: **James H. Bishop**, **Nolan Williams**, **David Spiegel**; Investigation: **James H. Bishop**, **Nolan Williams**, **David Spiegel**; Methodology: **James H. Bishop**, **Matthew D. Sacchet**; Project administration: **James H. Bishop, Heer Amin** ; Resources: **Matthew D. Sacchet**, **Hua Wu**, **Laima Baltusis**; Software: **Matthew D. Sacchet;** Supervision: **James H. Bishop**; Validation: **James H. Bishop**, **Andrew Geoly**; Visualization: **James H. Bishop** ; Writing – original draft: **James H. Bishop;** Writing – review & editing: **James H. Bishop**, **Matthew D. Sacchet, Poorvi Keshava.**

Declaration of Competing Interest

None.

Data availability

Data will be made available on request.

Acknowledgements

We would like to thank Meng Gu, Ph.D., Ralph Hurd, Ph.D., and Adam Kerr, Ph.D. for their assistance and expertise with MRI data collection as well as Keith Sudheimer, Ph.D. for providing functional MRI analysis support in the ancillary studies. Declarations of interest: none.

Appendix A. Supporting information

Supplementary data associated with this article can be found in the online version at doi:10.1016/j.jneumeth.2023.109853.

REFERENCES

Ashburner, J., Friston, K.J., 2005. Unified segmentation. Neuroimage 26 (3), 839–851.
Bai, X., Harris, A.D., Gong, T., Puts, N.A.J., Wang, G., Schar, M., Barker, P.B., Edden, R.A. E., 2017. Voxel placement precision for gaba-edited magnetic resonance spectroscopy. Open J. Radio. 7 (1), 35–44.
Bodenhausen, G., Freeman, R., Turner, D.L., 1969. Suppression of artifacts in two-dimensional J spectroscopy. Journal of Magnetic Resonance 1977;27(3):511–514.
Brodmann, K., 1909 Vergleichende Lokalisationslehre der Grosshirnrinde in ihren Prinzipien dargestellt auf Grund des Zellenbaues: Barth.
Cole, E.J., Stimpson, K.H., Bentzley, B.S., Gulser, M., Cherian, K., Tischler, C., Nejad, R., Pankow, H., Choi, E., Aaron, H., Espil, F.M., Pannu, J., Xiao, X., Duvio, D., Solvason, H.B., Hawkins, J., Guerra, A., Jo, B., Raj, K.S., Phillips, A.L., Barmak, F., Bishop, J.H., Coetzee, J.P., DeBattista, C., Keller, J., Schatzberg, A.F., Sudheimer, K. D., Williams, N.R., 2020. Stanford accelerated intelligent neuromodulation therapy for treatment-resistant depression. Am. J. Psychiatry 177 (8), 716–726.
Colin, S., David, John, H., Derek, L.G.H., 1998. Normalized entropy measure for multimodality image alignment. 1998.

Collignon, A., Maes, F., Delaere, D., Vandermeulen, D., Suetens, P., Marchal, G., 1995. Automated multi-modality image registration based on information theory. 1995.
Conover, W.J., Iman, R.L., 1981. Rank transformations as a bridge between parametric and nonparametric statistics. Am. Stat. 35 (3), 124–129.
Cox, R.W., 1996. AFNI: software for analysis and visualization of functional magnetic resonance neuroimages. Comput. Biomed. Res. 29 (3), 162–173.
Dice, L.R., 1945. Measures of the amount of ecologic association between species. Ecology 26 (3), 297–302.
von Economo, C.F., Koskinas, G.N., 1925. Die cytoarchitektonik der hirnrinde des erwachsenen menschen: J. Springer,.
Edden, R.A., Puts, N.A., Harris, A.D., Barker, P.B., Evans, C.J., 2014. Gannet: a batch-processing tool for the quantitative analysis of gamma-aminobutyric acid-edited MR spectroscopy spectra. J. Magn. Reson Imaging 40 (6), 1445–1452.
Faerman, A., Bishop, J.H., Stimpson, K.H., Phillips, A., Gülser, M., Amin, H., Nejad, R., DeSouza, D.D., Geoly, A.D., Kallioniemi, E., Jo, B., Williams, N.R., Spiegel, D., Modulation of a Stable Neurobehavioral Trait Using Repetitive Transcranial Magnetic Stimulation: A Preregistered Randomized Controlled Trial. medRxiv 2021: 2021.2007.2008.21260222.
Fischl, B., Salat, D.H., Busa, E., Albert, M., Dieterich, M., Haselgrove, C., van der Kouwe, A., Killiany, R., Kennedy, D., Klaveness, S., Montillo, A., Makris, N., Rosen, B., Dale, A.M., 2002. Whole brain segmentation: automated labeling of neuroanatomical structures in the human brain. Neuron 33 (3), 341–355.
Gasparovic, C., Song, T., Devier, D., Bockholt, H.J., Caprihan, A., Mullins, P.G., Posse, S., Jung, R.E., Morrison, L.A., 2006. Use of tissue water as a concentration reference for proton spectroscopic imaging. Magn. Reson. Med. 55 (6), 1219–1226.
Harris, A.D., Puts, N.A., Edden, R.A., 2015. Tissue correction for GABA-edited MRS: considerations of voxel composition tissue segmentation and tissue relaxations. J. Magn. Reson Imaging 42 (5), 1431–1440.
Hui, S.C.N., Mikkelsen, M., Zollner, H.J., Ahluwalia, V., Alcauter, S., Baltusis, L., Barany, D.A., Barlow, L.R., Becker, R., Berman, J.I., Berrington, A., Bhattacharyya, P.K., Blicher, J.U., Bogner, W., Brown, M.S., Calhoun, V.D., Castillo, R., Cecil, K.M., Choi, Y.B., Chu, W.C.W., Clarke, W.T., Craven, A.R., Cuypers, K., Dacko, M., de la Fuente-Sandoval, C., Desmond, P., Domagalik, A., Dumont, J., Duncan, N.W., Dydak, U., Dyke, K., Edmondson, D.A., Ende, G., Ersland, L., Evans, C.J., Fermin, A.S.R., Ferretti, A., Fillmer, A., Gong, T., Greenhouse, I., Grist, J.T., Gu, M., Harris, A.D., Hat, K., Heba, S., Heckova, E., Hegarty, J.P., 2nd , Heise, K.F., Jacobson, A., Jansen, J.F.A., Jenkins, C.W., Johnston, S.J., Juchem, C., Kangarlu, A., Kerr, A.B., Landheer, K., Lange, T., Lee, P., Levendovszky, S.R., Limperopoulos, C., Liu, F., Lloyd, W., Lythgoe, D.J., Machizawa, M.G., MacMillan, E.L., Maddock, R.J., Manzhurtsev, A. V., Martinez-Gudino, M.L., Miller, J.J., Mirzakhanian, H., Moreno-Ortega, M., Mullins, P.G., Near, J., Noeske, R., Nordhoy, W., Oeltzschner, G., Osorio-Duran, R., Otaduy, M.C.G., Pasaye, E.H., Peeters, R., Peltier, S.J., Pilatus, U., Polomac, N., Porges, E.C., Pradhan, S., Prisciandaro, J.J., Puts, N.A., Rae, C.D., Reyes-Madrigal, F., Roberts, T.P.L., Robertson, C.E., Rosenberg, J.T., Rotaru, D.G., O'Gorman Tuura, R.L., Saleh, M.G., Sandberg, K., Sangill, R., Schembri, K., Schrantee, A., Semenova, N.A., Singel, D., Sitnikov, R., Smith, J., Song, Y., Stark, C., Stoffers, D., Swinnen, S. P., Tain, R., Tanase, C., Tapper, S., Tegenthoff, M., Thiel, T., Thioux, M., Truong, P., van Dijk, P., Vella, N., Vidyasagar, R., Vovk, A., Wang, G., Westlye, L.T., Wilbur, T. K., Willoughby, W.R., Wilson, M., Wittsack, H.J., Woods, A.J., Wu, Y.C., Xu J., Lopez, M.Y., Yeung, D.K.W., Zhao, Q., Zhou, X., Zupan, G., Edden, R.A.E., Nakajima, S.L., Honda, S., 2021. Frequency drift in MR spectroscopy at 3T. Neuroimage ;241: 118430.
Hurd, R., Sailasuta, N., Srinivasan, R., Vigneron, D.B., Pelletier, D., Nelson, S.J., 2004. Measurement of brain glutamate using TE-averaged PRESS at 3T. Magn. Reson Med. 51 (3), 435–440.
Koush, Y., Elliott, M.A., Mathiak, K., 2011. Single voxel proton spectroscopy for neurofeedback at 7 Tesla. Materials 4.
Koush, Y., de Graaf, R.A., Jiang, L., Rothman, D.L., Hyder, F., 2019. Functional MRS with J-edited lactate in human motor cortex at 4T. Neuroimage 184, 101–108.
Mescher, M., Merkle, H., Kirsch, J., Garwood, M., Gruetter, R., 1998. Simultaneous in vivo spectral editing and water suppression. NMR Biomed. 11 (6), 266–272.
Oz, G., Deelchand, D.K., Wijnen, J.P., Mlynarik, V., Xin, L., Mekle, R., Noeske, R., Scheenen, T.W.J., Tkac, I., 2020. Experts' working group on advanced single voxel hm. advanced single voxel (1) h magnetic resonance spectroscopy techniques in humans: experts' consensus recommendations. NMR Biomed., e4236
Park, Y.W., Deelchand, D.K., Joers, J.M., Hanna, B., Berrington, A., Gillen, J.S., Kantarci, K., Soher, B.J., Barker, P.B., Park, H., Oz, G., Lenglet, C., 2018. AutoVOI: real-time automatic prescription of volume-of-interest for single voxel spectroscopy. Magn. Reson Med. 80 (5), 1787–1798.
Porges, E.C., Woods, A.J., Lamb, D.G., Williamson, J.B., Cohen, R.A., Edden, R.A.E., Harris, A.D., 2017. Impact of tissue correction strategy on GABA-edited MRS findings. Neuroimage 162, 249–256.
Press, W.H., Teukolsky, S.A., Vetterling, W.T., Flannery, B.P., 1992. Numerical recipes in C, 2nd ed..,. Cambridge University Press,.
Rajkowska, G., Goldman-Rakic, P.S., 1995. Cytoarchitectonic definition of prefrontal areas in the normal human cortex: II. variability in locations of areas 9 and 46 and relationship to the talairach coordinate system. Cereb. Cortex 5 (4), 323–337.
Sarkissov, S., Filimonoff, I., Kononowa, E., Preobraschenskaja, I., Kukuew, L., 1955. Atlas of the cytoarchitectonics of the human cerebral cortex. Moscow: Medgiz 1955;20.
Schur, R.R., Draisma, L.W., Wijnen, J.P., Boks, M.P., Koevoets, M.G., Joels, M., Klomp, D. W., Kahn, R.S., Vinkers, C.H., 2016. Brain GABA levels across psychiatric disorders: a systematic literature review and meta-analysis of (1) H-MRS studies. Hum. Brain Mapp. 37 (9), 3337–3352.
Shapiro, S.S., Wilk, M.B., 1965. An analysis of variance test for normality (complete samples)†. Biometrika 52 (3–4), 591–611.
SØRensen, T., 1948. A Method of establishing Groups of Equal Amplitude in Plant Sociology based on Similarity of Species Content, and its application to analyses of the vegetation on Danish commons. Pp. 34. København1948.
Stanley, J.A., Raz, N., 2018. Functional magnetic resonance spectroscopy: the "new" mrs for cognitive neuroscience and psychiatry research. Front. Psychiatry 9, 76.
Tran, T.K., Vigneron, D.B., Sailasuta, N., Tropp, J., Le Roux, P., Kurhanewicz, J., Nelson, S., Hurd, R., 2000. Very selective suppression pulses for clinical MRSI studies of brain and prostate cancer. Magn. Reson Med. 43 (1), 23–33.
Webb, P.G., Sailasuta, N., Kohler, S.J., Raidy, T., Moats, R.A., Hurd, R.E., 1994. Automated single-voxel proton MRS: technical development and multisite verification. Magn. Reson Med. 31 (4), 365–373.
Yasen, A.L., Smith, J., Christie, A.D., 2017. Reliability of glutamate and GABA quantification using proton magnetic resonance spectroscopy. Neurosci. Lett. 643, 121–124.